NeuroImage 70 (2013) 250–257

Contents lists available at SciVerse ScienceDirect

NeuroImage

journal homepage: www.elsevier.com/locate/ynimg

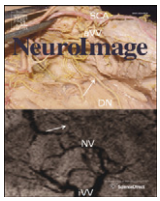

Decoding gender dimorphism of the human brain using multimodal anatomical and diffusion MRI data

Delia-Lisa Feis [a,*], Kay H. Brodersen [b,c], D. Yves von Cramon [a], Eileen Luders [d], Marc Tittgemeyer [a]

[a] Max Planck Institute for Neurological Research, Gleueler Straße 50, 50931 Cologne, Germany
[b] Translational Neuromodeling Unit, Institute for Biomedical Engineering, University of Zurich & ETH Zurich, Wilfriedstrasse 6, 8032 Zurich, Switzerland
[c] Department of Computer Science, ETH Zurich, Universitaetstrasse 6, 8092 Zurich, Switzerland
[d] Laboratory of Neuro Imaging, Department of Neurology, UCLA School of Medicine, Los Angeles, CA, USA

ARTICLE INFO

Article history:
Accepted 28 December 2012
Available online 5 January 2013

Keywords:
Gender dimorphism
Multivariate pattern analysis
Classification
Feature selection
Multimodal imaging
Decoding

ABSTRACT

The female brain contains a larger proportion of gray matter tissue, while the male brain comprises more white matter. Findings like these have sparked increasing interest in studying dimorphism of the human brain: the general effect of gender on aspects of brain architecture. To date, the vast majority of imaging studies is based on unimodal MR images and typically limited to a small set of either gray or white matter regions-of-interest. The morphological content of magnetic resonance (MR) images, however, strongly depends on the underlying contrast mechanism. Consequently, in order to fully capture gender-specific morphological differences in distinct brain tissues, it might prove crucial to consider multiple imaging modalities simultaneously. This study introduces a novel approach to perform such multimodal classification incorporating the relative strengths of each modality-specific physical aperture to tissue properties. To illustrate our approach, we analyzed multimodal MR images (T_1-, T_2-, and diffusion-weighted) from 121 subjects (67 females) using a linear support vector machine with a mass-univariate feature selection procedure. We demonstrate that the combination of different imaging modalities yields a significantly higher balanced classification accuracy (96%) than any one modality by itself (83%–88%). Our results do not only confirm previous morphometric findings; crucially, they also shed new light on the most discriminative features in gray-matter volume and microstructure in cortical and subcortical areas. Specifically, we find that gender disparities are primarily distributed along brain networks thought to be involved in social cognition, reward-based learning, decision-making, and visual-spatial skills.

Introduction

Sexual morphological differences in the human brain have attracted increasing interest in structural imaging analyses. A huge body of literature reveals sex differences in brain architecture. Postmortem studies (e.g. Witelson et al., 2006) as well as *in vivo* imaging studies (Filipek et al., 1994; Goldstein et al., 2001; Good et al., 2001) support the most robust finding of an approximately 10% larger total brain size in men. The female brain is known to contain a larger proportion of gray matter than the male brain, which, conversely, exhibits more white matter (Gur et al., 1999; Luders and Toga, 2010). It has been hypothesized that these differences in tissue volume contribute to difference in behavior (Gur et al., 1999). However, they cannot be the only determinant, since morphological differences remain even when controlling for brain size and tissue ratios (Luders et al., 2009). Findings like these hint at the critical effects of gender on brain architecture. Further research effort is encouraged by the difference in onset, prevalence and symptomatology of almost all neuropsychiatric illnesses between women and men (Giedd et al., 2012).

Structural imaging data have been predominantly analyzed using mass-univariate approaches, e.g., voxel-based morphometry (VBM; Davatzikos, 2004; Good et al., 2001), focusing on individual regions-of-interest. More recently, multivariate decoding approaches have been increasingly used as a powerful complement to mass-univariate approaches (Bendfeldt et al., 2012; Ecker et al., 2010; Klöppel et al., 2008; Lao et al., 2004; Pereira and Botvinick, 2011). It is currently unknown, however, whether multivariate approaches could be substantially enhanced by not only adopting a whole-brain perspective but by also simultaneously accounting for multiple modalities in a single statistical model.

To investigate this, we propose a multimodal analysis approach for structural classification that is characterized by three features. First, it is designed for whole-brain analyses and thus overcomes the limitations inherent in region-of-interest analyses. Second, we evaluate and visualize the importance of individual data features in discriminating between classes. Third, and most importantly, our approach integrates T_1-weighted, T_2-weighted and fractional anisotropy (FA) images.

Currently, the most widely used multivariate analysis is based on classification algorithms such as the support vector machine (SVM; Vapnik, 1998). An increasing number of studies have used SVMs to

* Corresponding author. Fax: +49 221 4726 298.
E-mail address: dfeis@nf.mpg.de (D.-L. Feis).

1053-8119/$ – see front matter © 2013 Elsevier Inc. All rights reserved.
http://dx.doi.org/10.1016/j.neuroimage.2012.12.068

obtain predictions about an individual diagnostic status, e.g., for Alzheimer's disease or mild cognitive impairment (Davatzikos et al., 2008; Klöppel et al., 2008; Teipel et al., 2007; Zhang et al., 2011). Other clinical examples include classification studies of schizophrenia (Koutsouleris et al., 2011), Turner syndrome (Marzelli et al., 2011), multiple sclerosis (Bendfeldt et al., 2012), or speech impairments in stroke patients (Brodersen et al., 2011).

Unlike previous classifiers, our approach is designed to exploit information jointly encoded by different acquisition modalities. It may particularly harvest interactions between anatomical structures that are differentially expressed in different image contrasts. Morphological group differences may in some cases be clearly visible from unimodal images alone; detecting large lesions of brain atrophy, for instance, is straightforward and unambiguous to the trained eye. Most neurological or psychiatric pathologies, by contrast, do not exhibit such clearly visible structural differences. Similarly, gender does not correlate with easily detectable structural differences. It is these cases that we expect to benefit most from a multivariate, multimodal approach. Thus, we analyzed 121 healthy subjects and decode gender from multimodal, structural MR images. In brief, our approach significantly outperformed all unimodal methods and led to novel findings about the spatial deployment of sexually discriminative features in the human brain.

Materials and methods

Subjects

A group of 121 right-handed volunteers (67 female, 54 male) with no history of neurological or psychiatric illness participated in the study. Handedness was determined by the Edinburgh handedness inventory (Oldfield, 1971) and did not differ significantly between females and males ($p = 0.69$; Wilcoxon rank sum test). A trained radiologist evaluated all T_1-weighted scans and assessed whether a subject can be considered as a normal healthy participant. Subjects were students ascertained from Cologne University and were between 20 and 30 years of age (mean: 25, SD: 2); there was no significant difference in age ($p = 0.41$; Wilcoxon rank sum test). All subjects gave informed consent, and the study was approved by the local ethics committee.

MRI data acquisition

High-resolution T_1- and T_2-weighted images were acquired using a Siemens 3 T Trio scanner (12-channel array head coil; maximum gradient strength 40 mT/m) with a whole-brain field of view (T_1-weighted: MDEFT3D; TR = 1930 ms, TI = 650 ms, TE = 5.8 ms, 128 sagittal slices, resolution = $1 \times 1 \times 1.25$ mm^3, flip angle = 18°; T_2-weighted: RARE; TR = 3200 ms, TE = 458 ms, 176 sagittal slices, resolution = $1 \times 1 \times 1$ mm^3). In addition, diffusion-weighted data (dMRI) were collected using spin-echo echo-planar imaging (twice refocused spin-EPI; TR = 9000 ms, TE = 87 ms, 72 axial slices, resolution = $1.7 \times 1.7 \times 1.7$ mm^3). Diffusion weighting was isotropically distributed along 60 directions (b-value 1000 s/mm^2). Finally, seven images without diffusion weighting were acquired at the beginning and after each block of ten diffusion-weighted images, providing an anatomical reference for motion correction. To increase the signal-to-noise ratio of the diffusion-weighted images, the arithmetic mean across three consecutive scanning sessions was computed. Altogether, these procedures resulted in a total scanning time of approximately 45 minutes.

Image preprocessing

T_1-weighted images were preprocessed using the VBM8 toolbox (http://dbm.neuro.uni-jena.de/vbm/) as described previously (Luders et al., 2009). Briefly, bias-field inhomogeneity was corrected and images were registered nonlinearly to a template derived from 550 healthy volunteers of the IXI database (http://www.brain-development.org/). Anatomical segmentation into the different tissue types, including gray matter (GM) and white matter (WM) was carried out using a *maximum a posteriori* (MAP) technique (Rajapakse et al., 1997), accounting for partial-volume effects (Tohka et al., 2004) and using a denoising method based on a hidden Markov random field model (Cuadra et al., 2005). In addition, deformation fields were computed during nonlinear registration.

For dMRI data, motion-correction parameters were estimated using all images with and without diffusion weighting from the three corresponding dMRI acquisitions. Fractional anisotropy (FA) values were estimated by fitting a diffusion tensor to the data within each voxel. FA images and T_2-weighted images were co-registered to T_1-weighted images. Subsequently, deformation fields were applied using the VBM8 toolbox in order to nonlinearly align the T_2-weighted and FA images to the template. GM and WM segments of T_1-weighted images were used to extract the analogs in T_2-weighted and FA images. Finally, tissue segments of T_1- and T_2-weighted images were smoothed using a Gaussian kernel (FWHM 3 mm; Jones and Cercignani, 2010).

Classification

In order to discriminate between female and male brains on the basis of multimodal images, we trained and tested a support vector machine (SVM, as implemented by Chang and Lin, 2011) with a linear kernel.

SVMs have proven to be simple and powerful tools in many previous studies, but they may overfit the data and make interpretation difficult when the number of features greatly exceeds the number of observations. This is because SVMs seek solutions that are sparse in examples but not sparse in features, and unlike Bayesian approaches they optimize the parameters rather than integrating out posterior uncertainty about them. We therefore included a feature-selection procedure to reduce the dimensionality of the feature space and discard non-informative dimensions in the data. In this way, we aimed to retain the simplicity and predictive power of a linear SVM while enforcing a small set of discriminative features, thus striking a balance between predictive power and interpretability of discriminative data features. Specifically, we used Fisher's criterion for feature selection (Furey et al., 2000), as described below.

Fisher's score considers the squared distance between class-conditional sample means $\hat{\mu}(\cdot)$ in relation to the respective intra-class sample standard deviations $\hat{\sigma}(\cdot)$,

$$f_v(X) = \frac{\left(\hat{\mu}(X^+) - \hat{\mu}(X^-)\right)^2}{\hat{\sigma}(X^+) + \hat{\sigma}(X^-)},$$

where the data $X = (X^+, X^-)$ are given by the signal intensities in a particular voxel v across all female (positive) and male (negative) subjects, respectively. We used this score to rank all features in terms of individual discriminative power (Müller et al., 2001). Voxels whose features were part of the upper 5th quantile of the resulting distribution of scores entered subsequent classification.

The utility of a classification model is typically assessed in terms of its substantive generalization performance on unseen data. Here, we estimated generalizability using a leave-one-subject-out cross-validation scheme. Within each fold, we optimized the misclassification hyperparameter C of the SVM using nested cross-validation on the current training set (Müller et al., 2004). In other words, we used an inner cross-validation loop for model selection and an outer loop for unbiased model evaluation. We repeated this analysis four times, using GM segments of either (i) T_1-weighted images, (ii) T_2-weighted images, (iii) FA images, or (iv) of all three images in combination (multimodal approach).

Classification performance was assessed using the balanced accuracy. In contrast to the conventional accuracy (i.e., the number of correctly classified subject labels divided by the number of subjects), the balanced

accuracy is defined as the arithmetic mean of the two accuracies obtained on positive and negative classes, respectively. The balanced accuracy provides an estimate of the probability of a correct prediction on future data where the unknown label has equal prior probability of coming from either class. This removes the bias that may arise in conventional sample accuracies when a classifier is trained and tested on an imbalanced dataset (Brodersen et al., 2010, 2012).

Since we used an SVM with a linear kernel, there is a direct correspondence between voxels and features. This makes it possible to interpret the distribution of weights in the original anatomical space and visualize the spatial deployment of informative voxels. In T_1-weighted GM maps, for example, voxel intensities reflect the amount of tissue within a particular region, while in FA maps voxel intensities represent the degree of anisotropy in each location. Since the classification problem addressed in this study is binary, a positive weight in the discrimination map indicates that, in this particular location, female subjects typically have higher voxel intensity than male subjects. Conversely, a negative weight means that voxel intensities tend to be higher in male than in female subjects. Thus, information from the estimated SVM model can be used to interpret classification results above and beyond predictive performance itself.

Results

Classification accuracy

In evaluating how well our approach was able to distinguish between female and male brains, we compared the classification performance on individual MR images with the performance on the combination of multiple modalities. We found that a multimodal approach provided both higher specificity and higher sensitivity (Fig. 1a) and thus enabled a significantly lower classification error than all unimodal approaches (Fig. 1b). While the most commonly used unimodal classifier (T_1-weighted GM) had a mean generalization error of 4.4%, our multimodal approach yielded an error of only 2.5% ($p<0.001$, $\alpha=0.01$; Mann–Whitney U test). For a numerical summary of these results, see Table 1.

The weakest classification performance (83% with a 95% credible interval of 75% to 88%) was achieved when using the FA GM segment only (Fig. 1c). Using T_2-weighted GM images led to a similar balanced accuracy (85% with a 95% credible interval of 77% to 90%). The highest performance within unimodal classifiers was achieved on the basis of T_1-weighted GM images (88% with a 95% credible interval of 80% to 92%). Notably, however, all of the above results were outperformed by the multimodal classifier ($p<0.01$, paired Wald test), which yielded a balanced accuracy of 96% (with a 95% credible interval of 89% to 98%).

Visualization of the decision boundary

To visualize the separability of subjects afforded by a multimodal classifier, we projected data features onto the weight vector of the SVM (Fig. 1d). This procedure highlights those male (4) and female (1) subjects that were misclassified. In absolute terms, 66 out of 67 women and 50 out of 54 men were assigned to the correct group.

Discrimination maps

In order to understand the spatial deployment of informative data features, we considered discrimination maps that are based on the weights attributed to each voxel by the SVM (Figs. 2–4). Regions

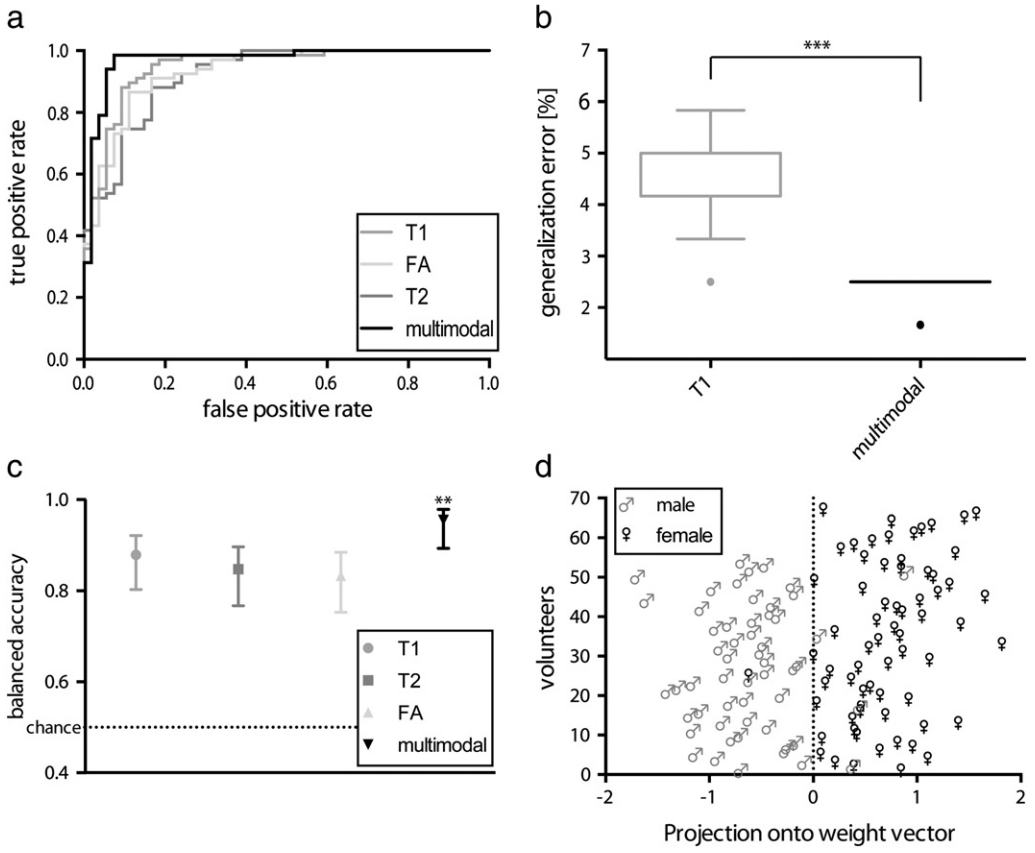

Fig. 1. Classification results. (a) Receiver operating characteristic (ROC) curves of the four classifiers evaluated in this study. (b) Boxplots of generalization error comparing the best unimodal (T_1-weighted) with the multimodal classifier. (c) Balanced classification accuracies with 95% central credible intervals. (d) Best classification accuracy (96%) provided by the multimodal classifier utilizing T_1-weighted, T_2-weighted and FA gray matter segments in combination. (** = significant, $p \leq 0.01$; *** = highly significant, $p<0.001$).

Table 1
Summary statistics of the four classifiers evaluated in this study.

Statistics	Multimodal	T_1	T_2	FA
Sensitivity	99%	93%	88%	93%
Specificity	93%	83%	82%	74%
Positive predictive value	94%	87%	86%	82%
Positive likelihood ratio	13.3	5.6	4.8	3.6
Area under the ROC curve	0.97	0.95	0.92	0.93

showing disparities between women and men were found in all four lobes, though primarily in the frontal lobe, with almost no differences occurring in the occipital lobe (Fig. 5). In cortical regions, some of these disparities appear lateralized to one hemisphere, while all subcortical differences are bilaterally distributed (Figs. 2, 4).

Relatively larger GM volumes in women as compared with men were found bilaterally in the anterior part of the superior frontal gyrus (BA 8/9), in the dorsolateral prefrontal cortex (BA 46), in the midcingulate cortex (BA 24), as well as subcortically in the ventromedial claustrum, in the ventral and medial parts of the caudate nucleus, in both hippocampi, and in the medial thalamus nuclei. Lateralized disparities between female and male subjects occurred predominantly in the orbitofrontal cortex (OFC), in the entorhinal cortex, in the anterior insular cortex, in the posterior part of superior temporal sulcus (pSTS), and in the temporoparietal junction area (TPJ). In these regions, women tended to show relatively larger GM volumes in the left lateral OFC (BA 47/12), left entorhinal cortex (BA 28), left anterior insular, left pSTS (BA 39), and left TPJ (BA 40), but also in right medial (BA 14) and basal (BA 13) OFC areas. Conversely, men exhibited relatively larger GM areas in the right lateral OFC (BA 47/12) and in the left OFC (BA 13), as well as in the right anterior insular cortex and in the right pSTS (Table 2).

Discussion

This paper presents a framework for whole-brain multivariate classification based on multiple MRI modalities, thus benefitting from distinct modality-specific physical apertures to different tissue properties. The main goal of this initial study was to determine whether this approach might substantially improve classification performance. As a proof of concept, we applied our method to analyze the sexual dimorphism of the human brain. Specifically, we employed a supervised machine-learning technique on MR images. To our knowledge, this is the first study investigating multimodal MR images using a multivariate pattern analysis approach for automated, whole-brain sex classification.

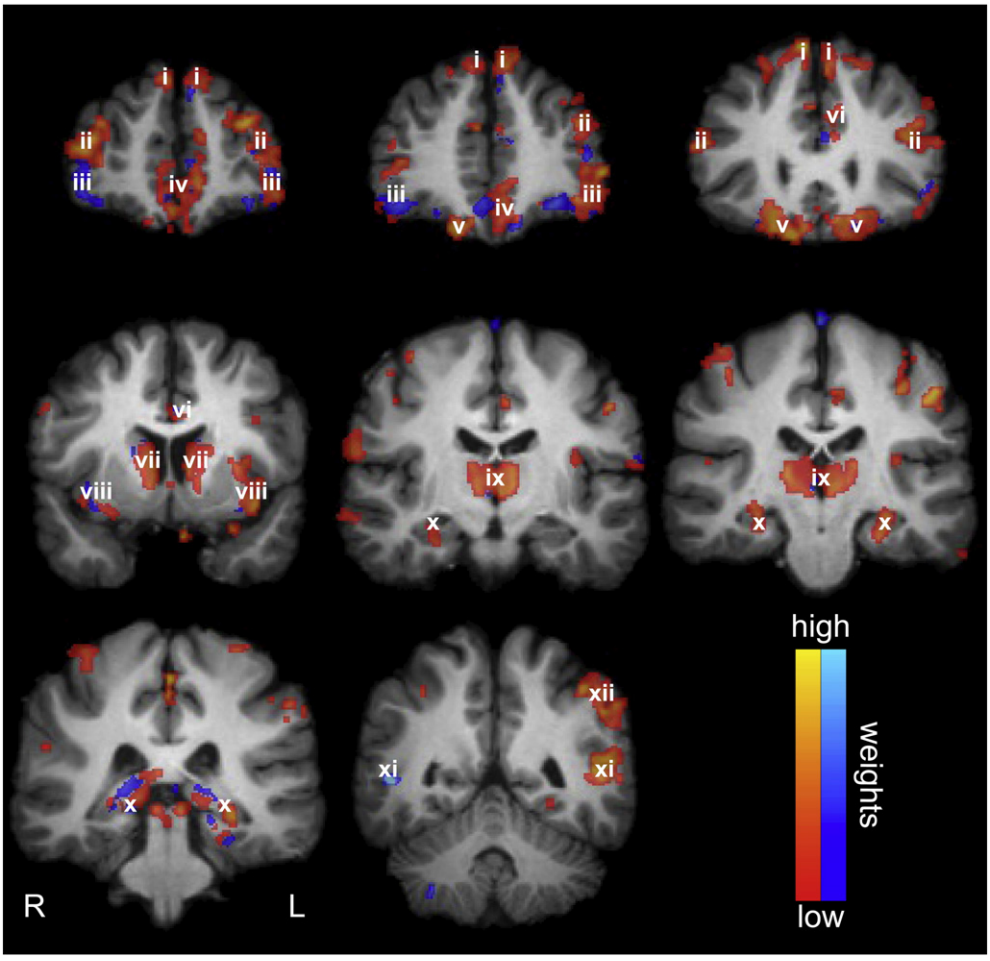

Fig. 2. Discrimination maps derived from gray matter segments of T_1-weighted images included in the multimodal classifier. Results are superimposed onto a T_1-weighted image of an individual study brain. To facilitate interpretation, a cluster-forming threshold of 27 voxels was used. The resulting regions comprise spatially contiguous patterns of relatively larger GM volume (positive weight vector; red color scale) or relatively smaller GM volume (negative weight vector; blue color scale) in women as compared to men, respectively. Labels: (i) anterior part of superior frontal gyrus, (ii) dorsolateral prefrontal cortex, (iii) lateral orbitofrontal cortex, (iv) medial orbitofrontal cortex/ventromedial prefrontal cortex, (v) orbitofrontal cortex, (vi) anterior midcingulate cortex, (vii) medial caudate nucleus, (viii) anterior insular cortex/claustrum, (ix) medial and posterior segment of the thalamus, (x) hippocampus, (xi) posterior division of superior temporal sulcus, and (xii) temporoparietal junction. L and R indicate the left and right hemispheres, respectively.

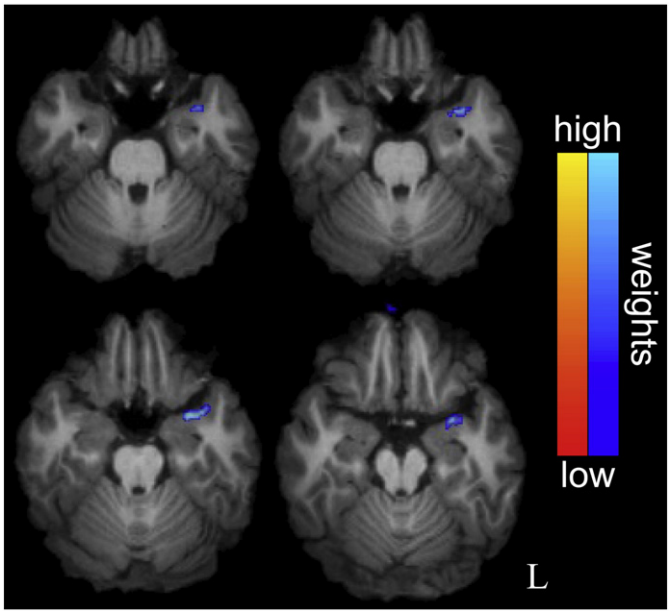

Fig. 3. Discrimination maps derived from gray matter segments of FA images included in the multimodal classifier, using the same procedure as in Fig. 2. The map shows one region with lower FA in male than female subjects (negative weight vector; blue color scale), representing a decreased diffusion anisotropy. Here, the major finding is a relatively higher FA of the left (L) entorhinal cortex in men (illustrated in blue).

Classification algorithm

Our approach combines multimodal images using a linear SVM which assigns a decision value to each subject, reflecting the distance between a given test subject's images and the hyperplane separating the two groups (Fig. 1d). The more ambiguous one sample is, the closer it is located at the hyperplane. Instead, a more prototypical test sample would lie further apart. Naturally, this also provides the possibility to construct a contingency table. Thus, we can directly derive numerical indicators such as sensitivity and specificity. Since we used a linear kernel, the components of the normal vector specifying the hyperplane can be interpreted in the space of the underlying neuroanatomical feature space.

Feature selection

Support vector machines have proven to be simple and powerful classification algorithms in many previous neuroimaging studies. However, they may overfit the data when, as is the case in multimodal MR images, the number of features exceeds the number of subjects by orders of magnitude. To overcome this limitation, we included a simple feature selection procedure in our approach. Specifically, we ranked all voxels according to their discriminative capacity using Fisher's criterion and admitted only a small fraction of top-ranking voxels to the classifier. Similar to Ecker et al. (2010) we found that keeping only 5% of all voxels resulted in the best classification performance. Notably, Ecker et al. (2010) used a recursive feature elimination algorithm, which iteratively came to the same conclusion as our one-step procedure. Thus, this approach is easy to implement and was found to enhance predictive performance substantially. Feature selection was embedded into a nested leave-one-subject-out cross-validation scheme to obtain an estimate of the generalization performance of the entire model that was not biased by the effects of feature selection. We used a Bayesian approach to performance evaluation by computing the posterior balanced accuracy for each classification result (Brodersen et al., 2010).

Classification results

Using the above framework, we analyzed the predictive capacity of four different feature spaces, including GM segments of either (i) T_1-weighted images, (ii) T_2-weighted images, (iii) FA images, or of (iv) all three images in combination (multimodal approach). We found that multimodal MR images outperformed all other feature spaces, yielding a significant reduction in classification error ($p<0.0001$; Mann–Whitney U test; Fig. 1b). Although all four

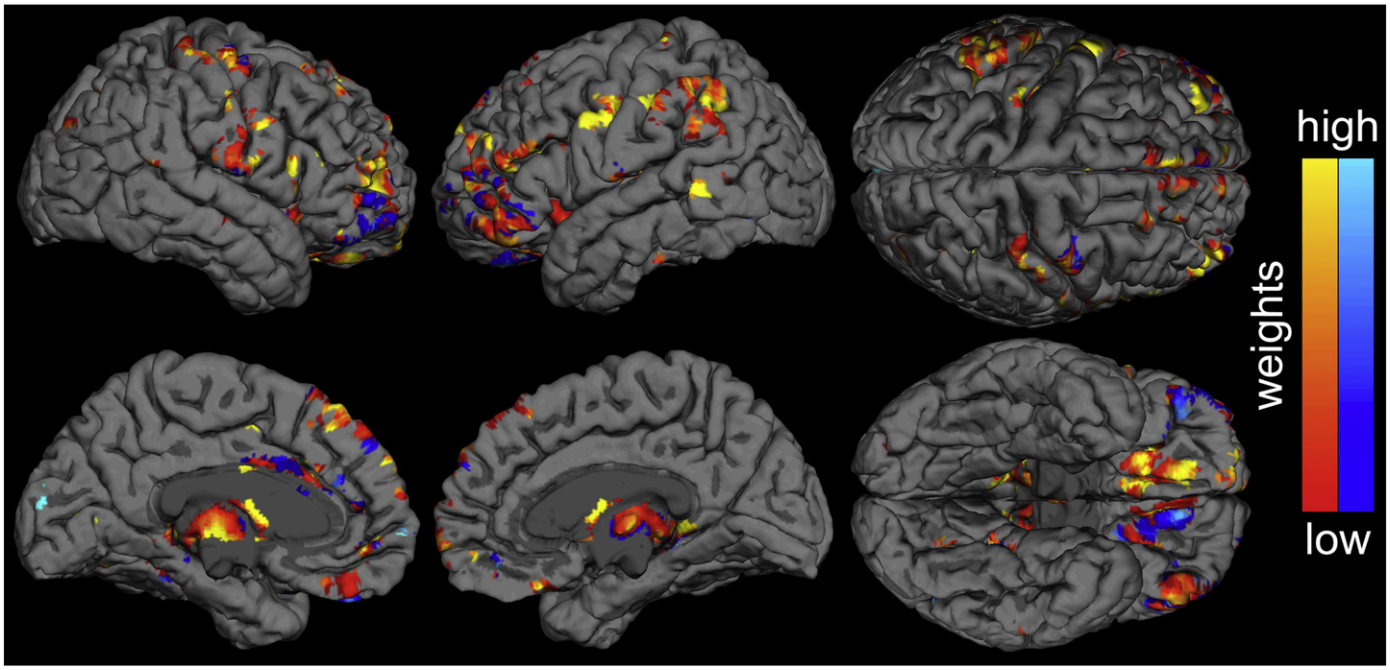

Fig. 4. Surface rendering of the discrimination maps shown in Fig. 2. First row: right and left lateral as well as the dorsal aspect. Second row: left and right mid-sagittal as well as ventral aspect. Relatively larger gray matter volumes in female than male subjects are shown in red, relatively smaller volumes in blue.

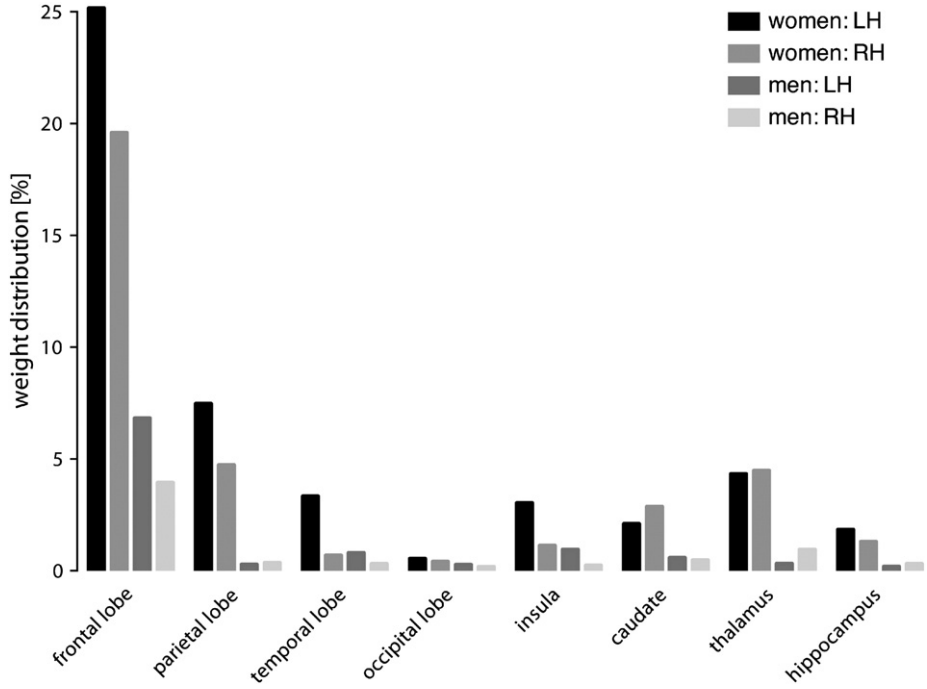

Fig. 5. Weighting distribution in cortical as well as subcortical regions found in T_1-weighted gray matter segments included in the multimodal classifier. Left (LH) and right (RH) hemispheres were distinguished and are represented in darker or brighter coloring, respectively.

classifiers performed well above chance (0.5), even the best unimodal classifier's balanced accuracy did not exceed 88% (Fig. 1c). By contrast, our multimodal approach enabled a balanced accuracy of 96% (with a 95% credible interval from 89% to 98%) and proved to be statistically significant ($p \leq 0.01$; paired Wald test). Thus, it clearly outperformed the other unimodal classifiers. Consistent with this result, we found that the ROC curve of our multimodal classifier showed higher sensitivity and higher specificity at nearly all classification thresholds (Fig. 1a). While the highest sensitivity and specificity in unimodal classification were 93% and 83%, respectively, our method performed its prediction with 99% sensitivity and 93% specificity. In terms of absolute numbers, our multimodal approach correctly classified 66 out of 67

Table 2
Overview of gray matter regions discriminating between women and men. Cluster labels correspond to indices in Fig. 2. Coordinates are given in MNI space and indicate, for each cluster, the location of its weight maximum. Abbreviations: SFG = superior frontal gyrus; DLPFC = dorsolateral prefrontal cortex; lOFC = lateral orbitofrontal cortex; mOFC = medial orbitofrontal cortex; MCC = midcingulate cortex; pSTS = posterior division of superior temporal sulcus; TPJ = temporoparietal junction; PIR = piriform lobe (entorhinal cortex); BA = Brodmann area.

Cluster	Region	Hemisphere	BA	MNI			Volume	Weight
				x (mm)	y(mm)	z(mm)	mm^3	
i	SFG	Left	8/9	−8	38	50	1937	11.54
		Right		8	29	60	1725	12.87
ii	DLPFC	Left	46	−33	54	24	3429	13.66
		Right		35	56	15	3632	11.77
iii	lOFC	Left	47/12	−53	41	0	3392	11.95
		Right		45	45	−17	1664	−6.85
iv	mOFC	Right	14	5	62	−9	4968	9.61
v	OFC	Left	13	−27	41	−17	1029	−7.08
		Right		12	26	−29	3378	14.96
vi	MCC	Left	24	0	−5	27	368	9.87
vii	Caudate Ncl	Left		−6	11	3	1617	7.70
		Right		8	9	2	2228	7.09
viii	Insular cortex	Left		−39	8	−14	2494	9.71
		Right		39	6	−5	111	−2.93
ix	Thalamus	Left		−18	−32	−2	5198	8.42
x	Hippocampus	Left		−29	−38	−8	1769	11.57
		Right		32	−23	−20	493	7.60
xi	pSTS	Left	39	−50	−48	12	1225	10.69
		Right		51	−53	3	105	−13.00
xii	TPJ	Left	40	−32	−77	29	1185	11.31
	PIR	Left	28	−29	2	−24	273	15.62

women and 50 out of 54 men (Fig. 1d). Initially, we wanted to include FA WM segments to get an insight into WM disparities, but we found that the inclusion of FA GM segments contributed most to the prediction of men.

Neuroanatomical findings

One of the key features of our approach is its potential for neuroanatomical interpretation that goes beyond the conclusions that can be derived from unimodal classifiers. Specifically, we found several neuroanatomical differences in spatially distributed cortical and subcortical patterns that differed between women and men (Figs. 3–5). Crucially, because our approach is multivariate, it does not rely on individual voxels being discriminative by themselves. Rather, our approach enables us to detect combinations of voxels that are jointly informative about gender. Put more simply, the resulting discriminative regions may be predictive of gender either because of their large between-group differences in volume or because their inter-regional correlations differ between classes. Regarding the former, two kinds of patterns can be distinguished: regions with relatively larger volume in female subjects as compared with males (red color scale, Figs. 2–4) and areas with relatively larger volume in male subjects as compared to females (blue color scale).

The gray matter segments of the T_1-weighted images included in the multimodal approach revealed a marked anterior–posterior gradient in classifier weights (Fig. 4) in conjunction with a remarkable lateralization in cortical regions (Fig. 5). In contrast, subcortical disparities were distributed rather bilaterally. Strikingly, the anterior–posterior gradient is dominated by differences in the frontal lobe. There were virtually no disparities in postcentral parts of the brain with the exception of TPJ and pSTS. Interestingly, Allen et al. (2003) already described the occipital lobe as the least sexually dimorphic region since they found no significant difference in gray matter volumes in females and males. They argue that most of this brain region has relatively low levels of sex steroid receptors (Goldstein et al., 2001). By contrast, disparities in the frontal lobe were found in all aspects of prefrontal areas, i.e., in the medial, lateral as well as orbital parts. Based on sex steroid receptor density, Goldstein et al. (2001) predicted that the prefrontal regions as well as the parietal cortices should exhibit a high degree of sexual dimorphism. Our findings with respect to contributing brain networks might be suggestive of sex differences in terms of social cognition, reward-based learning, decision-making, and visual-spatial skills. The effects observed within the right and left nuclei caudate also corroborate previous observations (Giedd et al., 1996; Good et al., 2001; Luders et al., 2009).

Interestingly though, while previous studies have primarily reported proportionately more gray matter in women rather than in men (reviewed in Luders and Toga, 2010), our approach also allowed us to identify regions that seem indicative of the opposite effect. More specifically, although receiving lower weights on average (Fig. 5), we detected several regions that showed relatively more gray matter in male than in female brains. These regions included the right anterior insular cortex, the right lateral as well as the left OFC (Figs. 2 and 4), and the right pSTS (Fig. 2). Relatively higher FA values in men as compared to women were found in the left entorhinal cortex (Fig. 3), indicating differences in cortical microstructure. It has long been known that efferent fibers exiting the piriform lobe primarily target the mOFC, the lOFC as well as the hippocampus. We found all of these regions to differ between women and men.

Conclusions

In summary, using sex differences as an illustrative example, the multimodal classification approach presented in this paper allowed us to substantially improve the prediction performance of previously described unimodal schemes. In addition, our results did not only confirm well-known sex differences previously reported in the literature; but they also proved to be sufficiently sensitive in separating women and men while identifying biologically plausible networks with maximal discriminative power. Overall, our study confirms that supervised machine-learning techniques possess the capacity of detecting even subtle and spatially distributed morphological differences. We envisage that such approaches may aid the clinical diagnosis of neurological as well as psychiatric pathologies that express differential neuroanatomical features.

Acknowledgments

This study was funded by the German Research Foundation in the Clinical Research Group 219 (MT) and the German Ministry of Education and Research (DLF; Grant 01GW0772).

Author contributions: DLF, KHB and MT designed the research; DLF contributed analytic tools, DLF analyzed data; EL and DYC contributed specific knowledge; DLF and MT wrote the paper.

The authors declare no conflict of interest.

References

Allen, J.S., Damasio, H., Grabowski, T.J., Bruss, J., Zhang, W., 2003. Sexual dimorphism and asymmetries in the gray-white composition of the human cerebrum. NeuroImage 18, 880–894.

Bendfeldt, K., Klöppel, S., Nichols, T.E., Smieskova, R., Kuster, P., Traud, S., Mueller-Lenke, N., Naegelin, Y., Kappos, L., Radue, E.-W., Borgwardt, S.J., 2012. Multivariate pattern classification of gray matter pathology in multiple sclerosis. NeuroImage 60, 400–408.

Brodersen, K.H., Mathys, C., Chumbley, J.R., Daunizeau, J., 2012. Bayesian mixed-effects inference on classification performance in hierarchical datasets. J. Mach. Learn. Res. 13, 3133–3176.

Brodersen, K.H., Ong, C.S., Stephan, K.E., Buhmann, J.M., 2010. The balanced accuracy and its posterior distribution. Pattern Recognition (ICPR), 2010 20th International Conference on, pp. 3121–3124.

Brodersen, K.H., Schofield, T.M., Leff, A.P., Ong, C.S., Lomakina, E.I., Buhmann, J.M., Stephan, K.E., 2011. Generative embedding for model-based classification of fMRI data. PLoS Comput. Biol. 7, e1002079.

Chang, C.C., Lin, C.J., 2011. LIBSVM: a library for support vector machines. ACM Trans. Intell. Syst. Technol. 2, 27.

Cuadra, M.B., Cammoun, L., Butz, T., Cuisenaire, O., Thiran, J.-P., 2005. Comparison and validation of tissue modelization and statistical classification methods in T1-weighted MR brain images. IEEE Trans. Med. Imaging 24, 1548–1565.

Davatzikos, C., 2004. Why voxel-based morphometric analysis should be used with great caution when characterizing group differences. NeuroImage 23, 17–20.

Davatzikos, C., Fan, Y., Wu, X., Shen, D., Resnick, S.M., 2008. Detection of prodromal Alzheimer's disease via pattern classification of magnetic resonance imaging. Neurobiol. Aging 29, 514–523.

Ecker, C., Rocha-Rego, V., Johnston, P., Mourao-Miranda, J., Marquand, A., Daly, E.M., Brammer, M.J., Murphy, C., Murphy, D.G., Consortium, M.A., 2010. Investigating the predictive value of whole-brain structural MR scans in autism: a pattern classification approach. NeuroImage 49, 44–56.

Filipek, P.A., Richelme, C., Kennedy, D.N., Caviness, V.S., 1994. The young adult human brain: an MRI-based morphometric analysis. Cereb. Cortex 4, 344–360.

Furey, T.S., Cristianini, N., Duffy, N., Bednarski, D.W., Schummer, M., Haussler, D., 2000. Support vector machine classification and validation of cancer tissue samples using microarray expression data. Bioinformatics 16, 906–914.

Giedd, J.N., Raznahan, A., Mills, K.L., Lenroot, R.K., 2012. Review: magnetic resonance imaging of male/female differences in human adolescent brain anatomy. Biol. Sex Differ. 3, 19.

Giedd, J.N., Snell, J.W., Lange, N., Rajapakse, J.C., Casey, B.J., Kozuch, P.L., Vaituzis, A.C., Vauss, Y.C., Hamburger, S.D., Kaysen, D., Rapoport, J.L., 1996. Quantitative magnetic resonance imaging of human brain development: ages 4–18. Cereb. Cortex 6, 551–560.

Goldstein, J.M., Seidman, L.J., Horton, N.J., Makris, N., Kennedy, D.N., Caviness, V.S., Faraone, S.V., Tsuang, M.T., 2001. Normal sexual dimorphism of the adult human brain assessed by in vivo magnetic resonance imaging. Cereb. Cortex 11, 490–497.

Good, C.D., Johnsrude, I., Ashburner, J., Henson, R.N., Friston, K.J., Frackowiak, R.S., 2001. Cerebral asymmetry and the effects of sex and handedness on brain structure: a voxel-based morphometric analysis of 465 normal adult human brains. NeuroImage 14, 685–700.

Gur, R.C., Turetsky, B.I., Matsui, M., Yan, M., Bilker, W., Hughett, P., Gur, R.E., 1999. Sex differences in brain gray and white matter in healthy young adults: correlations with cognitive performance. J. Neurosci. 19, 4065–4072.

Jones, D.K., Cercignani, M., 2010. Twenty-five pitfalls in the analysis of diffusion MRI data. NMR Biomed. 23, 803–820.

Klöppel, S., Stonnington, C.M., Chu, C., Draganski, B., Scahill, R.I., Rohrer, J.D., Fox, N.C., Jack, C.R., Ashburner, J., Frackowiak, R.S.J., 2008. Automatic classification of MR scans in Alzheimer's disease. Brain 131, 681–689.

Koutsouleris, N., Davatzikos, C., Bottlender, R., Patschurek-Kliche, K., Scheuerecker, J., Decker, P., Gaser, C., Möller, H.-J., Meisenzahl, E.M., 2011. Early recognition and disease prediction in the at-risk mental states for psychosis using neurocognitive pattern classification. Schizophr. Bull. 38, 1200–1215.

Lao, Z., Shen, D., Xue, Z., Karacali, B., Resnick, S.M., Davatzikos, C., 2004. Morphological classification of brains via high-dimensional shape transformations and machine learning methods. NeuroImage 21, 46–57.
Luders, E., Gaser, C., Narr, K.L., Toga, A.W., 2009. Why sex matters: brain size independent differences in gray matter distributions between men and women. J. Neurosci. 29, 14265–14270.
Luders, E., Toga, A.W., 2010. Sex differences in brain anatomy. Prog. Brain Res. 186, 3–12.
Marzelli, M.J., Hoeft, F., Hong, D.S., Reiss, A.L., 2011. Neuroanatomical spatial patterns in Turner syndrome. NeuroImage 55, 439–447.
Müller, K.-R., Krauledat, M., Dornhege, G., Curio, G., Blankertz, B., 2004. Machine Learning Techniques for Brain–Computer Interfaces.
Müller, K.-R., Mika, S., Rätsch, G., Tsuda, K., Schölkopf, B., 2001. An introduction to kernel-based learning algorithms. IEEE Trans. Neural Networks 12, 181–201.
Oldfield, R.C., 1971. The assessment and analysis of handedness: the Edinburgh inventory. Neuropsychologia 9, 97–113.
Pereira, F., Botvinick, M., 2011. Information mapping with pattern classifiers: a comparative study. NeuroImage 56, 476–496.
Rajapakse, J.C., Giedd, J.N., Rapoport, J.L., 1997. Statistical approach to segmentation of single-channel cerebral MR images. IEEE Trans. Med. Imaging 16, 176–186.
Teipel, S.J., Born, C., Ewers, M., Bokde, A.L.W., Reiser, M.F., Möller, H.-J., Hampel, H., 2007. Multivariate deformation-based analysis of brain atrophy to predict Alzheimer's disease in mild cognitive impairment. NeuroImage 38, 13–24.
Tohka, J., Zijdenbos, A., Evans, A., 2004. Fast and robust parameter estimation for statistical partial volume models in brain MRI. NeuroImage 23, 84–97.
Vapnik, V.N., 1998. Statistical Learning Theory. Wiley-Interscience.
Witelson, S.F., Beresh, H., Kigar, D.L., 2006. Intelligence and brain size in 100 postmortem brains: sex, lateralization and age factors. Brain 129, 386–398.
Zhang, D., Wang, Y., Zhou, L., Yuan, H., Shen, D., Initiative, A.a.s.D.N., 2011. Multimodal classification of Alzheimer's disease and mild cognitive impairment. NeuroImage 55, 856–867.